Measurement of the $^{18}O(\alpha,\gamma)^{22}Ne$ Reaction Rate at JUNA and Its Impact on Probing the Origin of SiC Grains

L. H. Wang,[1] J. Su,[1,*] Y. P. Shen,[2,†] J. J. He,[1] M. Lugaro,[3,4,5,6,‡] B. Szányi,[3,4,7] A. I. Karakas,[6,8] L. Y. Zhang,[1] X. Y. Li,[1] B. Guo,[2] G. Lian,[2] Z. H. Li,[2] Y. B. Wang,[2] L. H. Chen,[2] B. Q. Cui,[2] X. D. Tang,[9] B. S. Gao,[9] Q. Wu,[9] L. T. Sun,[9] S. Wang,[10] Y. D. Sheng,[1] Y. J. Chen,[1] H. Zhang,[1] Z. M. Li,[1] L. Y. Song,[1] X. Z. Jiang,[1] W. Nan,[2] W. K. Nan,[2] L. Zhang,[2] F. Q. Cao,[2] T. Y. Jiao,[9] L. H. Ru,[9] J. P. Cheng,[1] M. Wiescher,[11,12] and W. P. Liu[2,13,§]

[1]*Key Laboratory of Beam Technology of Ministry of Education, College of Nuclear Science and Technology, Beijing Normal University, Beijing 100875, China*

[2]*China Institute of Atomic Energy, P. O. Box 275(10), Beijing 102413, China*

[3]*Konkoly Observatory, Research Centre for Astronomy and Earth Sciences (CSFK), Eötvös Loránd Research Network (ELKH), Konkoly Thege Miklós út 15-17, 1121 Budapest, Hungary*

[4]*CSFK, MTA Centre of Excellence, Budapest, Konkoly Thege Miklós út 15-17, H-1121, Hungary*

[5]*ELTE Eötvös Loránd University, Institute of Physics, Budapest 1117, Pázmány Péter sétány 1/A, Hungary*

[6]*School of Physics and Astronomy, Monash University, Victoria 3800, Australia*

[7]*Graduate School of Physics, University of Szeged, Dom tér 9, Szeged, 6720 Hungary*

[8]*ARC Centre of Excellence for All Sky Astrophysics in 3 Dimensions (ASTRO 3D), Australia*

[9]*Institute of Modern Physics, Chinese Academy of Sciences, Lanzhou 730000, China*

[10]*Shandong Provincial Key Laboratory of Optical Astronomy and Solar-Terrestrial Environment, Institute of Space Sciences, Shandong University, Weihai 264209, China*

[11]*Department of Physics and The Joint Institute for Nuclear Astrophysics, University of Notre Dame, Notre Dame, Indiana 46556-5670, USA*

[12]*Wolfson Fellow of Royal Society, School of Physics and Astronomy, University of Edinburgh, King's Buildings, Edinburgh EH9 3FD, United Kingdom*

[13]*College of Science, Southern University of Science and Technology, Shenzhen 518055, China*

(Received 27 June 2022; revised 22 September 2022; accepted 13 January 2023; published 2 March 2023)

The $^{18}O(\alpha,\gamma)^{22}Ne$ reaction is critical for AGB star nucleosynthesis due to its connection to the abundances of several key isotopes, such as ^{21}Ne and ^{22}Ne. However, the ambiguous resonance energy and spin-parity of the dominant 470 keV resonance leads to substantial uncertainty in the $^{18}O(\alpha,\gamma)^{22}Ne$ reaction rate for the temperature of interest. We have measured the resonance energies and strengths of the low-energy resonances in $^{18}O(\alpha,\gamma)^{22}Ne$ at the Jinping Underground Nuclear Astrophysics experimental facility (JUNA) with improved precision. The key 470 keV resonance energy has been measured to be $E_\alpha = 474.0 \pm 1.1$ keV, with such high precision achieved for the first time. The spin-parity of this resonance state is determined to be 1^-, removing discrepancies in the resonance strengths in earlier studies. The results significantly improve the precision of the $^{18}O(\alpha,\gamma)^{22}Ne$ reaction rates by up to about 10 times compared with the previous data at typical AGB temperatures of 0.1–0.3 GK. We demonstrate that such improvement leads to precise ^{21}Ne abundance predictions, with an impact on probing the origin of meteoritic stardust SiC grains from AGB stars.

DOI: 10.1103/PhysRevLett.130.092701

Asymptotic giant branch (AGB) stars represent the final phases of the evolution of stars with initial mass roughly 1 to 8 $M_\odot$ during which H and He burning occur alternately [1]. The production of free neutrons during He burning leads to the *slow* neutron capture process (*s*-process) producing approximately half of the abundances of the nuclei between Fe and Bi [2]. In AGB stars of relatively low mass, between roughly 1.5 and 4 $M_\odot$, $^{13}C(\alpha,n)^{16}O$ is the main neutron source. The neutron flux from $^{22}Ne(\alpha,n)^{25}Mg$ affects only the abundances of the isotopes of the intermediate mass elements from Si to Ni, and of the isotopes heavier than iron affected by branching points on the *s*-process path. In more massive AGB stars, instead, the He-shell temperatures are higher and the $^{22}Ne(\alpha,n)^{25}Mg$ reaction is more efficiently activated, also contributing to the bulk production of the elements heavier than iron [3–5]. The latter neutron source is also activated during core He burning in massive supergiant stars, such as Betelgeuse. There, neutron captures drive the production of the elements from Fe to Sr [6]. Both in AGB and supergiant stars, the ^{22}Ne neutron source isotope is produced via the reaction chain $^{14}N(\alpha,\gamma)^{18}F(\beta^+\upsilon)^{18}O(\alpha,\gamma)^{22}Ne$. The $^{18}O(\alpha,\gamma)^{22}Ne$

reaction, therefore, represents the crucial link that allows the conversion of ^{14}N into ^{22}Ne and the subsequent production of neutrons. As a result, the $^{18}O(\alpha,\gamma)^{22}Ne$ reaction rate is a key parameter to accurately and precisely determine the ^{22}Ne abundance and the subsequent $^{22}Ne(\alpha,n)^{25}Mg$ neutron production rate.

During He burning, there are also other nucleosynthetic channels, which are marginal relative to the main α-capture chain described above, but crucial for the production of specific isotopes in the He-rich shell (hereafter "intershell") of AGB stars. These channels can be more or less activated starting on ^{18}O also depending on the relative ratio of their rates and that of $^{18}O(\alpha,\gamma)^{22}Ne$. In particular, the $^{18}O(\alpha,n)^{21}Ne$ reaction affects the final abundance of ^{21}Ne (e.g., [7]). The isotope is especially interesting because there are observational constraints for it. ^{21}Ne data are provided from the analysis of noble gases in meteoritic stardust SiC grains that originated in AGB stars.

However, at the typical temperature range 0.1–0.3 GK of helium burning in AGB stars, the $^{18}O(\alpha,\gamma)^{22}Ne$ reaction rates suffer from large uncertainties, which mainly come from the ambiguous resonance energy and strength of the 470 keV resonance. Up to now, only two experiments have measured the resonance energy using transfer reactions, 470 ± 18 keV via $^{18}O(^6Li,d)^{22}Ne$ [8] and 495 ± 12 keV via $^{20}Ne(t,p)^{22}Ne$ [9]. Since the resonance energy is on the exponential term in the calculation, even small variations in the energy can bring significant uncertainty to the reaction rates. For example, the reaction rate will increase ≈240% at 0.1 GK by changing the resonance energy from 495 to 470 keV. Therefore, it is crucial to clarify the current disagreement on the resonance energy via a new experiment with high precision.

There was a significant inconsistency in the resonance strengths. Based on the spectroscopic factor presented in Ref. [8], Käppeler *et al.* [10] deduced an inconclusive resonance strength to be $\omega\gamma_{470} = 0.55$ μeV(0^+) or 0.23 μeV(1^-) suffering from the ambiguous spin parity [8]. In 2003, Dababneh *et al.* [11] measured the $^{18}O(\alpha,\gamma)^{22}Ne$ reaction via the γ-γ coincidence method, obtaining an $\omega\gamma_{470} = 0.48 \pm 0.16$ μeV by assuming a 50% branching ratio for the γ transition via the 1274 keV state in ^{22}Ne. Very recently, Dombos *et al.* [12] reported the first direct underground measurement of this reaction in CASPAR underground facility and gave a new resonance strength $\omega\gamma_{470} = 0.26 \pm 0.05$ μeV. It can be seen that the good determinations of the spin-parity and γ-ray branching ratios of the 470 keV resonance state are also essential to obtain reliable $^{18}O(\alpha,\gamma)^{22}Ne$ reaction rates.

In this Letter, we present the results of a direct measurement of the $^{18}O(\alpha,\gamma)^{22}Ne$ reaction at the Jinping Underground Nuclear Astrophysics experimental facility (JUNA) [13]. The critical 470 keV resonance energy is precisely determined for the first time by direct measurement. Furthermore, we derive primary γ-ray branching ratios and then determine the spin-parity of the 470 keV resonance state, which resolves the resonance strength discrepancy. Based on our new data on the resonances, we report the most precise reaction rates at the temperature range of helium burning.

The measurement was performed at the 400 kV accelerator of JUNA in the China Jinping Underground Laboratory (CJPL) [14]. In this work, the γ rays emitted from $^{18}O(\alpha,\gamma)^{22}Ne$ were detected by a nearly 4π BGO detector array composed of eight identical segments with an energy resolution of 12%@662 keV. An experimental setup similar to previous works [15,16] is adopted. The ^{18}O-enriched (98% abundance) gas is used to produce the $Ti^{18}O_x$ (x is the atom ratio of oxygen to titanium) targets by filter cathodic vacuum arc (FCVA) technology [17]. By measuring the yield curve of the 151 keV resonance in $^{18}O(p,\gamma)^{19}F$, the atom ratio of oxygen to titanium of the target is determined to be 1.76 ± 0.09. The degradation of the target is measured to be 6% after 94 Coulomb $^4He^{2+}$ irradiation by monitoring the maximum yield of the 660 keV resonance.

The $^4He^{2+}$ beam is accelerated with energy from 470 to 787 keV to scan the yield curves of the low energy $^{18}O(\alpha,\gamma)^{22}Ne$ resonances. The typical $^4He^{2+}$ beam intensity is approximately 500 eμA. To calibrate the energy of the accelerator and the stoichiometry of the target, a proton beam with energy from 147 to 369 keV is applied to scan the yield curves of the 151 and 334 keV resonances in $^{18}O(p,\gamma)^{19}F$. The energy of the accelerator is calibrated by the 151 and 334 keV resonances in $^{18}O(p,\gamma)^{19}F$ and the 660, 750, and 770 keV resonances in $^{18}O(\alpha,\gamma)^{22}Ne$. In the calibration, the benchmarks are $E_{lab} = 151.3 \pm 0.3$ [18] and 334.1 ± 1.3 keV [19,20] for the resonances in $^{18}O(p,\gamma)^{19}F$ and are $E_{lab} = 661.7 \pm 1.0$, 750.2 ± 1.0, and 767.7 ± 1.0 keV for the resonances in $^{18}O(\alpha,\gamma)^{22}Ne$, which are the weighted averages of the results reported in previous direct measurements [21,22]. Figure 1 shows the thick target yield curve of the 470 keV $^{18}O(\alpha,\gamma)^{22}Ne$ resonance, in which the yields are calculated by the counts of the sum peak (9550–10 550 keV) in the sum spectrum representing the sum of the energies of all eight BGO segments. The 50% point of the front edge of the fitting curve [23], $E_{lab} = 474.0 \pm 1.1$ keV, is adopted as the resonance energy and indicated in Fig. 1. The uncertainty comes from (i) energy calibration of the accelerator (0.6 keV); (ii) the energy loss of the beam in the deposited carbon on the target's surface estimated with the yield of $^{12}C(p,\gamma)^{13}N$ (0.8 keV). The energy loss of the beam is 1.6 keV at 474 keV, and then half of this energy loss is adopted as uncertainty considering the roughness of the deposited carbon layer; (iii) the yield curve's fitting (0.4 keV). This result produces an excitation energy of $E_x = 10\,054.6 \pm 0.9$ keV to the 470 keV resonance state combing with a Q value of 9666.82 ± 0.02 keV [24], which is the most precise value and the first result

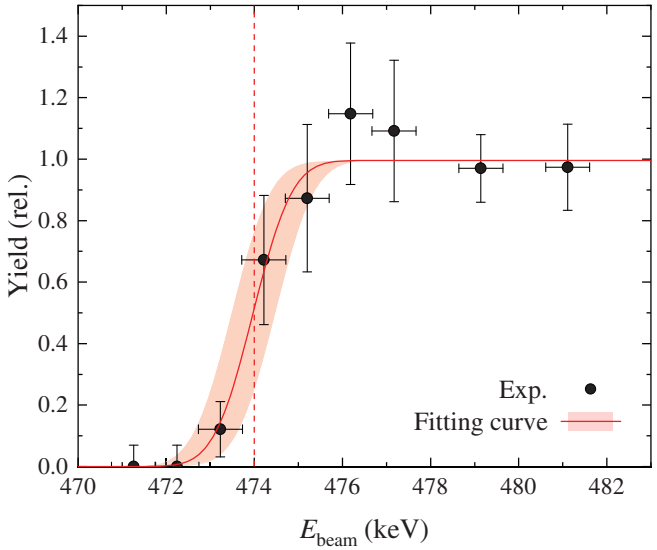

FIG. 1. Thick target yield curve of the 470 keV resonance in $^{18}O(\alpha,\gamma)^{22}Ne$. The solid red line is the fitting curve, the red shadow represents the uncertainty of the fitting curve, and the dashed red line marks the position of resonance energy. All yields are normalized to the maximum yield of the fitting curve.

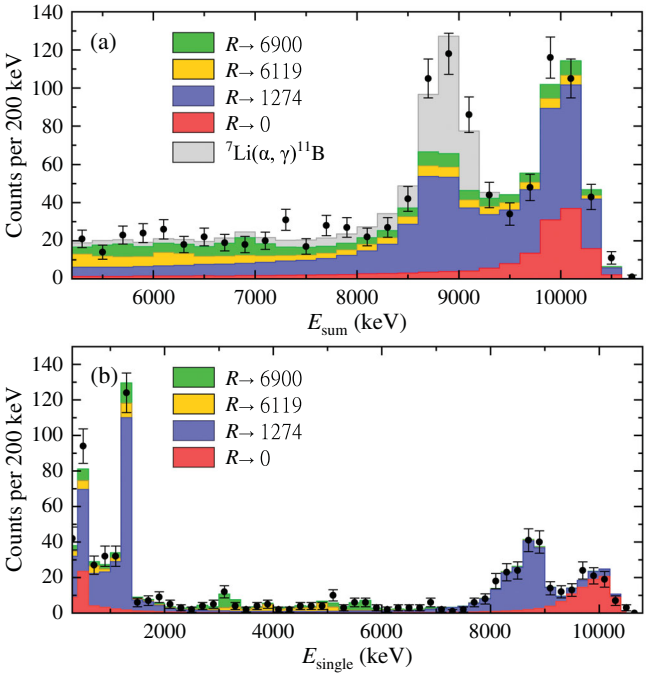

FIG. 2. (a) Sum spectra of the 470 keV resonance after subtracting the background. (b) Single spectra produced by putting a 9550–10 550 keV gate on the sum peak shown in (a). The different color areas represent the fractional contribution.

determined by direct measurement. Compared with the values adopted in previous works [11,12,25,26], the precision of the 470 keV resonance energy is improved by more than an order of magnitude, which greatly reduces the uncertainty in the $^{18}O(\alpha,\gamma)^{22}Ne$ reaction rate.

The γ spectra obtained for the 470 keV resonance are shown in Fig. 2: Figure 2(a) shows the sum spectrum. Figure 2(b) shows the single spectrum, which is obtained by superimposing the spectra of eight BGO segments by putting a 9550–10 550 keV gate on the sum peak shown in Fig. 2(a). The corresponding spectra measured below the resonance are adopted as the background and subtracted.

The primary γ-ray branching ratios of the 470 keV resonance are extracted by fitting the sum and single spectra obtained using the Bayesian Analysis Toolkit (BAT) [27], in which the fractional contribution to the spectra of each primary γ-transition and the subsequent transitions are produced by Monte Carlo simulation with the Geant4 toolkit [28]. The peak around 8900 keV in the sum spectrum cannot be reproduced if only the contribution of $^{18}O(\alpha,\gamma)^{22}Ne$ is considered. The excess is found to be caused by the $E_{lab} = 401$ keV $^{7}Li(\alpha,\gamma)^{11}B$ resonance [29] when the $^{4}He^{2+}$ beam bombard on the ^{7}Li contaminant in the Ta substrate by analyzing the yield curve of this peak, which is supported by the ^{7}Li profile obtained by the secondary ion mass spectroscopy (SIMS) analysis of the target after the beam irradiation [30]. Moreover, the ^{7}Li content in the Ta substrate is estimated to be 0.5×10^{-5} by the maximum yield of the $E_{lab} = 401$ keV $^{7}Li(\alpha,\gamma)^{11}B$ resonance, which is consistent with the 1.2×10^{-5} of a pure Ta target deduced by measuring the yield of $^{7}Li(p,\gamma)^{8}Be$ at $E_{lab} = 390$ keV. According to the energy resolution of the detector, the contribution from 8900 keV peak to the sum peak of $^{18}O(\alpha,\gamma)^{22}Ne$ can be neglected. The fitting results show four contributions from the R → 0, 1274, 5146, 6900 keV transitions. The corresponding primary γ-ray branching ratios are $(17 \pm 4)\%$, $(55 \pm 10)\%$, $(13 \pm 4)\%$, and $(15 \pm 5)\%$, respectively. The direct transition to the ground states (0^+) in ^{22}Ne rule out the 0^+ possibility of the resonance state. Therefore, a 1^- spin-parity has been firmly assigned to the 10 054.6 keV state, in combination with the previous study [8].

The resonance strength is calculated by the relative method used in Ref. [15] as

$$\omega\gamma = \frac{\lambda_R^2(R)}{\lambda_R^2}\frac{\epsilon_{eff}}{\epsilon_{eff}(R)}\frac{N(R)}{N}\frac{A_{sum}/\eta_{sum}}{A_{sum}(R)/\eta_{sum}(R)}\omega\gamma(R), \quad (1)$$

in which λ_R and ϵ_{eff} are the de Broglie wavelength and the effective stopping power of the beam in the target at the particular resonance energy evaluated in the laboratory frame, respectively. N is the beam particle number. A_{sum} and η_{sum} are the count and detection efficiency of the sum peak, respectively. R represents the reference resonance. The 151 keV resonance in $^{18}O(p,\gamma)^{19}F$ is adopted as the reference due to its large yield. The weighted average $\omega\gamma_{151} = 0.98 \pm 0.03$ meV of previous results [18,22,31–34] is adopted. The resonance strengths of the five low-energy resonances in $^{18}O(\alpha,\gamma)^{22}Ne$ are determined and

TABLE I. Resonance energies and resonance strengths obtained in this Letter for the $^{18}O(\alpha,\gamma)^{22}Ne$ reaction and compared with those of previous works.

E_α (keV)				$\omega\gamma$ (μeV)					
JUNA	Ref. [21]	Ref. [22]	Ref. [12]	JUNA	Ref. [21]	Ref. [22]	Ref. [10]	Ref. [11]	Ref. [12]
474.0 ± 1.1[a]			472 ± 18[b]	0.25 ± 0.03			$0.55(0^+)$ $0.23(1^-)$	0.48 ± 0.16	0.26 ± 0.05
573 ± 9[c]			569 ± 15[b]	0.62 ± 0.10				0.71 ± 0.17	0.63 ± 0.30
661.7 ± 1.0[d]	656 ± 4	662.1 ± 1.0		202 ± 17	290 ± 50	230 ± 25		229 ± 19	225 ± 12
750.2 ± 1.0[d]	755 ± 4	749.9 ± 1.0		500 ± 44	390 ± 70	560 ± 60		490 ± 40	553 ± 34
767.7 ± 1.0[d]	769 ± 4	767.6 ± 1.0		1093 ± 99		1200 ± 120			1306 ± 77

[a]Obtained in this work.
[b]Calculated the resonance energies using the excitation energy in Table 3 of Ref. [8].
[c]Dombos *et al.* [12] recommends a resonance energy of $E_{lab} = 569 \pm 15$ keV, which slightly deviates from the value of $E_{lab} = 573 \pm 9$ keV adopted by [25]. As this resonance energy is not determined in the present work, we adopt the value from Iliadis *et al.* [25].
[d]Weighted average of the results reported in previous direct measurements [21,22].

listed in Table I. The main sources of uncertainty are (i) the uncertainty of the effective stopping power ratio $\epsilon_{eff}/\epsilon_{eff}(151)$ caused by the O to Ti ratio inhomogeneity of the target; (ii) statistical errors associated with counts of the sum peak and beam particle; (iii) the uncertainty in the reference resonance strength; and (iv) the uncertainty in the sum peak efficiency ratio caused by branching ratios fitting.

The present result of $\omega\gamma_{470} = 0.25 \pm 0.03$ μeV shows good agreement with the $\omega\gamma_{470} = 0.26 \pm 0.05$ μeV obtained in the most recent underground direct measurement [12], as well as the $\omega\gamma_{470} = 0.23$ μeV [10] predicted for the 1^- spin-parity assignment. Based on the primary γ-ray branching ratios obtained here, the branching ratio of the 1274 keV γ ray is deduced to be 83%, which modifies the results of Ref. [11] to $\omega\gamma_{470} = 0.29 \pm 0.10$ μeV. Thus, all 470 keV resonance strength results now show agreement by using the primary γ-ray branching ratios obtained in this work. The other resonance strengths obtained also show good agreement with those reported in previous works [11,12].

Table II lists the $^{18}O(\alpha,\gamma)^{22}Ne$ reaction rates calculated using the RatesMC code [35] with the parameters listed in Table I. Figure 3 shows a comparison of the present reaction rates (JUNA) with those reported by Angulo *et al.* [26] (NACRE) and Iliadis *et al.* [36] (Iliadis10). The JUNA reaction rate is much lower than the NACRE rate, mostly due to the new 470 keV resonance strength, and close to the Iliadis10's rate because the discrepancies in the resonance strength and energy cancel each other. Thanks to our new data for the 470 keV resonance, the precision of the $^{18}O(\alpha,\gamma)^{22}Ne$ reaction rates in the 0.1–0.3 GK range are significantly improved by up to about 10 times compared with the previous data [26,36]. For example, at $T = 0.2$ GK, the uncertainty of the JUNA rate is $^{+13}_{-11}$%, much lower than the previous $^{+172}_{-47}$% [26] and $^{+79}_{-42}$% [36].

We analyzed the astrophysical impact of the new $^{18}O(\alpha,\gamma)^{22}Ne$ reaction rates in the context of He burning in AGB stars by calculating the abundances of ^{21}Ne in the intershell of AGB stellar models from Ref. [37] of two masses (2 and 3 $M_\odot$) and solar metallicity 0.014 [38]. It is possible to precisely measure the $^{21}Ne/^{22}Ne$ ratio in the meteoritic stardust SiC grains via mass spectrometry [39], see Fig. 4, where a selection of the data is presented. Note that the model predictions should not be compared to the actual data, but to the bottom-left end of the regression lines through the data. In fact, the grain data do not represent completely pure He-shell composition because we cannot exclude a small amount of mixing with envelope material (of "Normal" ≃ solar, composition). Therefore,

TABLE II. The total reaction rates of $^{18}O(\alpha,\gamma)^{22}Ne$ in units of $cm^3\ mol^{-1}\ s^{-1}$.

T_9	Low rate	Median rate	High rate
0.07	2.64×10^{-26}	3.16×10^{-25}	1.41×10^{-24}
0.08	8.68×10^{-25}	9.67×10^{-24}	4.32×10^{-23}
0.09	5.87×10^{-23}	1.79×10^{-22}	6.69×10^{-22}
0.1	5.68×10^{-21}	7.22×10^{-21}	1.13×10^{-20}
0.11	2.70×10^{-19}	3.16×10^{-19}	3.71×10^{-19}
0.12	7.00×10^{-18}	8.10×10^{-18}	9.36×10^{-18}
0.13	1.11×10^{-16}	1.28×10^{-16}	1.47×10^{-16}
0.14	1.18×10^{-15}	1.36×10^{-15}	1.56×10^{-15}
0.15	9.16×10^{-15}	1.05×10^{-14}	1.20×10^{-14}
0.16	5.48×10^{-14}	6.26×10^{-14}	7.16×10^{-14}
0.18	1.09×10^{-12}	1.24×10^{-12}	1.41×10^{-12}
0.2	1.24×10^{-11}	1.39×10^{-11}	1.57×10^{-11}
0.25	1.33×10^{-09}	1.44×10^{-09}	1.56×10^{-09}
0.3	4.50×10^{-08}	4.78×10^{-08}	5.08×10^{-08}
0.35	6.77×10^{-07}	7.16×10^{-07}	7.58×10^{-07}
0.4	5.56×10^{-06}	5.86×10^{-06}	6.20×10^{-06}
0.45	2.92×10^{-05}	3.07×10^{-05}	3.25×10^{-05}
0.5	1.10×10^{-04}	1.16×10^{-04}	1.23×10^{-04}
0.6	8.08×10^{-04}	8.51×10^{-04}	8.97×10^{-04}
0.7	3.30×10^{-03}	3.47×10^{-03}	3.66×10^{-03}
0.8	9.32×10^{-03}	9.83×10^{-03}	1.04×10^{-02}
0.9	2.07×10^{-02}	2.18×10^{-02}	2.30×10^{-02}
1	3.91×10^{-02}	4.12×10^{-02}	4.34×10^{-02}

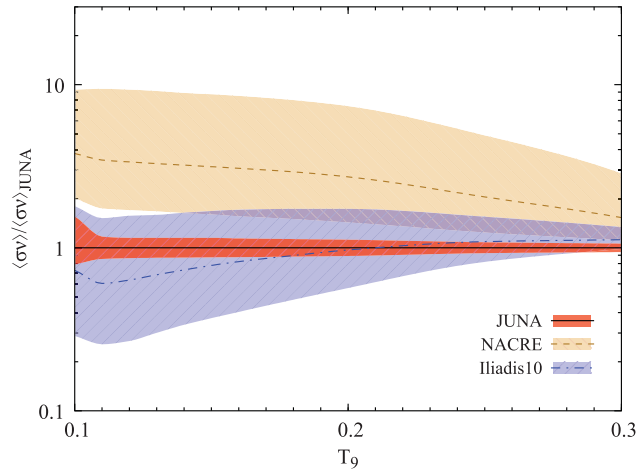

FIG. 3. Comparison of the present $^{18}O(\alpha,\gamma)^{22}Ne$ reaction rates (JUNA) with previous values reported by Angulo *et al.* [26] (NACRE) and Iliadis *et al.* [36] (Iliadis10).

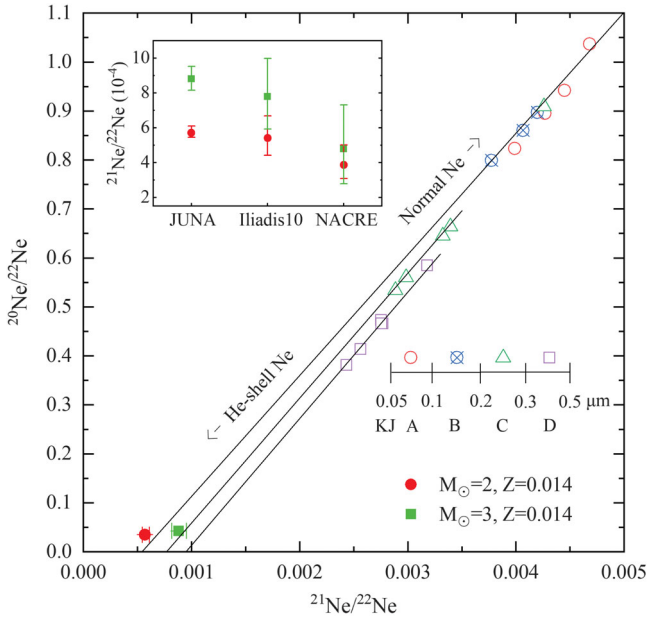

FIG. 4. Ne isotopic ratios predicted in the intershell of different AGB models (filled symbols) using the JUNA $^{18}O(\alpha,\gamma)^{22}Ne$ reaction rates and those observed in meteoritic stardust SiC grains of different sizes Lewis *et al.* [39] (open symbols), in which error bars only represent the contribution from the $^{18}O(\alpha,\gamma)^{22}Ne$ reaction rates. The symbol legend is at the bottom-right side of the plot. (See Fig. 8 of Lewis *et al.* [39] and Fig. 2 of Karakas *et al.* [7] from similar figures). The three regression lines are fits to the KJB, KJC, and KJD samples representing the mixing between material of normal composition ($\simeq$ solar, located at the top-right outside the plot boundaries) and of AGB He-shell composition (located at the bottom left). When comparing the observed and predicted AGB He-shell composition with find an agreement of the models with the smallest size samples. The top-left inset shows the $^{21}Ne/^{22}Ne$ ratios calculated with different $^{18}O(\alpha,\gamma)^{22}Ne$ reaction rates.

the regression lines represent such mixed composition, and the models represent the pure He-shell component. As the error bars on the data points are typically less than 1%, the regression lines are determined very precisely [39]. Therefore, even tiny variations in the predictions are significant. The JUNA precise reaction rate significantly decreases the uncertainty from the $^{18}O(\alpha,\gamma)^{22}Ne$ reaction on the predicted $^{21}Ne/^{22}Ne$ ratio: from ~30% using the Iliadis10's rate, down to ~8%, as shown in the inset in Fig. 4. This improvement increases the effectiveness of using the $^{21}Ne/^{22}Ne$ ratio to constraint the mass of the parent AGB stars of SiC grains of different sizes—other uncertainties, such as those from other reaction rates and input stellar model parameters, still need to be investigated.

In summary, we have measured the resonance energies and strengths of the low-energy resonances in $^{18}O(\alpha,\gamma)^{22}Ne$ using a BGO array detector at the JUNA facility. We have precisely determined the resonance energy of the key 470 keV resonance to be $E_{lab} = 474.0 \pm 1.1$ keV for the first time via direct measurement. We also determined the primary γ branching ratios of the 470 keV resonance. The observed direct $R \to 0^+$ transition establish a 1^- spin-parity assignment to the 10 054.6 keV state in ^{22}Ne, removing discrepancies in the resonance strengths claimed in earlier studies. Based on our experimental results, the precision of the $^{18}O(\alpha,\gamma)^{22}Ne$ reaction rates in the 0.1–0.3 GK range are significantly improved by up to about 10 times compared with the previous data. The new reaction rates have allowed us to provide more accurate and precise predictions of the ^{21}Ne abundances in the intershell of AGB stars. The comparison of the predicted $^{21}Ne/^{22}Ne$ ratio and that measured in stardust SiC grains provides a stricter constraint on the masses of the AGB parent stars of the grains, improving the possibility of probing the origin of the stardust SiC grains of different sizes.

The authors thank the staff of the CJPL and Yalong River Hydropower Development Company and Tsinghua University for the laboratory support. The present work is supported by the National Natural Science Foundation of China (Grants No. 11490560, No. U1867211, No. 12275026, No. 12222514, No. 12005304, No. 12125509, and No. 11775133), the National Key R&D Program of China (Grant No. 2022YFA1603300 and No. 2022YFA1602301), the CAST Young Talent Support Plan, and the CNNC Science Fund for Talented Young Scholars. A. I. K. was supported by the Australian Research Council Centre of Excellence for All Sky Astrophysics in 3 Dimensions (ASTRO 3D), through Project No. CE170100013. M. W. was supported as a Wolfson Fellow of the Royal Society, at the University of Edinburgh, UK.

*sujun@bnu.edu.cn
†ypshen@ciae.ac.cn
‡maria.lugaro@csfk.org
§wpliu@ciae.ac.cn; liuwp@sustech.edu.cn

[1] A. I. Karakas and J. C. Lattanzio, Pub. Astron. Soc. Aust. **31**, e030 (2014).
[2] C. Sneden, J. J. Cowan, and R. Gallino, Annu. Rev. Astron. Astrophys. **46**, 241 (2008).
[3] M. Lugaro, F. Herwig, J. C. Lattanzio, R. Gallino, and O. Straniero, Astrophys. J. **586**, 1305 (2003).
[4] M. A. van Raai, M. Lugaro, A. I. Karakas, D. A. García-Hernández, and D. Yong, Astron. Astrophys. **540**, A44 (2012).
[5] S. Cristallo, O. Straniero, L. Piersanti, and D. Gobrecht, Astrophys. J. Suppl. Ser. **219**, 40 (2015).
[6] M. Pignatari, R. Gallino, M. Heil, M. Wiescher, F. Käppeler, F. Herwig, and S. Bisterzo, Astrophys. J. **710**, 1557 (2010).
[7] A. I. Karakas, H. Y. Lee, M. Lugaro, J. Görres, and M. Wiescher, Astrophys. J. **676**, 1254 (2008).
[8] U. Giesen, C. Browne, J. Görres, J. Ross, M. Wiescher *et al.*, Nucl. Phys. **A567**, 146 (1994).
[9] Z. Q. Mao and H. T. Fortune, Phys. Rev. C **50**, 2116 (1994).
[10] F. Käppeler, M. Wiescher, U. Giesen, J. Görres, I. Baraffe *et al.*, Astrophys. J. **437**, 396 (1994).
[11] S. Dababneh, M. Heil, F. Käppeler, J. Görres, M. Wiescher, R. Reifarth, and H. Leiste, Phys. Rev. C **68**, 025801 (2003).
[12] A. C. Dombos, D. Robertson, A. Simon, T. Kadlecek, M. Hanhardt *et al.*, Phys. Rev. Lett. **128**, 162701 (2022).
[13] W. Liu, Z. Li, J. He, X. Tang, G. Lian *et al.*, Sci. China Phys. Mech. Astron. **59**, 642001 (2016).
[14] J. Cheng, K. J. Kang, J. Li, J. Li, Y. Li *et al.*, Annu. Rev. Nucl. Part. Sci. **67**, 231 (2017).
[15] J. Su, H. Zhang, Z. Li, P. Ventura, Y. Li *et al.*, Sci. Bull. **67**, 125 (2022).
[16] L. Zhang, J. Su, J. He, M. Wiescher, R. deBoer *et al.*, Phys. Rev. Lett. **127**, 152702 (2021).
[17] L. Wang, Y. Shen, J. Su, X. Li, W. Yan *et al.*, Nucl. Instrum. Methods Phys. Res., Sect. B **512**, 49 (2022).
[18] A. Best, F. Pantaleo, A. Boeltzig, G. Imbriani, M. Aliotta *et al.*, Phys. Lett. B **797**, 134900 (2019).
[19] D. Tilley, H. Weller, C. Cheves, and R. Chasteler, Nucl. Phys. **A595**, 1 (1995).
[20] M. Wang, W. Huang, F. G. Kondev, G. Audi, and S. Naimi, Chin. Phys. C **45**, 030003 (2021).
[21] H. Trautvetter, M. Wiescher, K.-U. Kettner, C. Rolfs, and J. Hammer, Nucl. Phys. **A297**, 489 (1978).
[22] R. B. Vogelaar, T. R. Wang, S. E. Kellogg, and R. W. Kavanagh, Phys. Rev. C **42**, 753 (1990).
[23] W. A. Fowler, C. Lauritsen, and T. Lauritsen, Rev. Mod. Phys. **20**, 236 (1948).
[24] M. Wang, G. Audi, F. G. Kondev, W. Huang, S. Naimi, and X. Xu, Chin. Phys. C **41**, 030003 (2017).
[25] C. Iliadis, R. Longland, A. Champagne, and A. Coc, Nucl. Phys. **A841**, 251 (2010).
[26] C. Angulo, M. Arnould, M. Rayet, P. Descouvemont, D. Baye *et al.*, Nucl. Phys. **A656**, 3 (1999).
[27] A. Caldwell, D. Kollar, and K. Kröninger, Comput. Phys. Commun. **180**, 2197 (2009).
[28] S. Agostinelli, J. Allison, K. a. Amako, J. Apostolakis, H. Araujo *et al.*, Nucl. Instrum. Methods Phys. Res., Sect. A **506**, 250 (2003).
[29] G. Hardie, B. W. Filippone, A. J. Elwyn, M. Wiescher, and R. E. Segel, Phys. Rev. C **29**, 1199 (1984).
[30] See Supplemental Material at http://link.aps.org/supplemental/10.1103/PhysRevLett.130.092701 for analysis of the background at 8.9 MeV peak in the sum spectrum of the 470 keV resonance.
[31] M. Wiescher, H. Becker, J. Görres, K.-U. Kettner, H. Trautvetter *et al.*, Nucl. Phys. **A349**, 165 (1980).
[32] H. Becker, W. Kieser, C. Rolfs, H. Trautvetter, and M. Wiescher, Z. Phys. A **305**, 319 (1982).
[33] J. Dermigny, C. Iliadis, M. Buckner, and K. Kelly, Nucl. Instrum. Methods Phys. Res., Sect. A **830**, 427 (2016).
[34] F. R. Pantaleo, A. Boeltzig, A. Best, R. Perrino, M. Aliotta *et al.*, Phys. Rev. C **104**, 025802 (2021).
[35] R. Longland, C. Iliadis, A. Champagne, J. R. Newton, C. Ugalde *et al.*, Nucl. Phys. **A841**, 1 (2010).
[36] C. Iliadis, R. Longland, A. Champagne, A. Coc, and R. Fitzgerald, Nucl. Phys. **A841**, 31 (2010).
[37] A. I. Karakas and M. Lugaro, Astrophys. J. **825**, 26 (2016).
[38] M. Asplund, N. Grevesse, A. J. Sauval, and P. Scott, Annu. Rev. Astron. Astrophys. **47**, 481 (2009).
[39] R. S. Lewis, S. Amari, and E. Anders, Geochim. Cosmochim. Acta **58**, 471 (1994).